

UC Davis

UC Davis Previously Published Works

Title

Hydroxylation of ZnO/Cu(1 1 1) inverse catalysts under ambient water vapor and the water-gas shift reaction

Permalink

<https://escholarship.org/uc/item/9bn874zt>

Journal

Journal of Physics D, 52(45)

ISSN

0022-3727

Authors

Orozco, Ivan
Huang, Erwei
Gutiérrez, Ramón A
et al.

Publication Date


2019-11-06

DOI

10.1088/1361-6463/ab37da

Peer reviewed

Hydroxylation of ZnO/Cu(1 1 1) inverse catalysts under ambient water vapor and the water–gas shift reaction

Ivan Orozco¹, Erwei Huang¹, Ramón A Gutiérrez², Zongyuan Liu³, Feng Zhang⁴, Mausumi Mahapatra³, Jindong Kang¹, Heath Kersell⁵, Slavomir Nemsak⁵, Pedro J Ramírez², Sanjaya D Senanayake³, Ping Liu^{1,3} and José A Rodríguez^{1,3,4,6} 

¹ Department of Chemistry, SUNY at Stony Brook, Stony Brook, New York 11794, United States of America

² Facultad de Ciencias, Universidad Central de Venezuela, Caracas 1020-A, Venezuela

³ Chemistry Department, Brookhaven National Laboratory, Upton, New York 11973, United States of America

⁴ Department of Materials Science and Engineering, SUNY at Stony Brook, Stony Brook, New York 11794, United States of America

⁵ Advanced Light Source, Lawrence Berkeley National Laboratory, Berkeley, CA 94720, United States of America

E-mail: rodriguez@bnl.gov

Abstract

The interaction of water vapor with ZnO/CuO_x/Cu(1 1 1) surfaces was investigated using synchrotron-based ambient pressure x-ray photoelectron spectroscopy (AP-XPS) and density-functional theory (DFT) calculations. Cu(1 1 1) does not dissociate the water molecule.

Cleavage of O–H bonds was seen with AP-XPS after depositing ZnO or preparing CuO_x on the copper substrate. The results of DFT calculations show unique behavior for ZnO/CuO_x/Cu(1 1 1), not seen on Cu(1 1 1), CuO_x/Cu(1 1 1) or ZnO(000 $\bar{1}$). The ZnO/CuO_x/Cu(1 1 1) system binds water quite well and exhibits the lowest energy barrier for O–H bond cleavage. The presence of unsaturated Zn cations in the islands of ZnO led to high chemical reactivity. In order to remove the OH from ZnO/CuO_x/Cu(1 1 1) and ZnO/Cu(1 1 1) surfaces, heating to elevated temperatures was necessary. At 500–600 K, a significant coverage of OH groups was still present on the surfaces and did react with CO during the water–gas shift (WGS) process. The final state of the sample depended strongly on the amount of ZnO present on the catalyst surface. For surfaces with a ZnO coverage below 0.3 ML, the adsorption of water did not change the integrity of the ZnO islands. On the other hand, for surfaces with a ZnO coverage above 0.3 ML, a ZnO \rightarrow Zn_xOH transformation was observed. This transformation led to a decrease in the WGS catalytic activity.

⁶ Author to whom any correspondence should be addressed.

1. Introduction

Oxide-oxide interfaces are at the core of heterogeneous catalysis [1]. Catalysts which contain a CuO–ZnO mixture are frequently used for the water–gas shift, the hydrogenation of CO or CO₂ to oxygenates, CO oxidation, methane conversion, and the destruction of pollutants such as NO or SO₂ [1–5]. A major goal is to optimize the configuration of industrial catalysts to make use of the intrinsic properties of oxide-oxide interfaces [1, 6–8]. The activity of the catalyst will depend on how the different elements in the system are combined [6–8]. Deposition of an oxide at submonolayer amounts over a second oxide host can create nanostructures which in turn may enhance the overall catalytic properties of the entire system [6–8]. The size and high density of defects in oxide nanoparticles can lead to special electronic, chemical and catalytic properties [7–9]. Images of high-resolution transmission electron microscopy (HRTEM) show overlayers of ZnO on top of Cu or CuO_x particles present in Cu/ZnO/Al₂O₃ catalysts utilized for the conversion of CO/CO₂ to CH₃OH [3, 10, 11]. The zinc oxide overlayers exhibited a graphite-like structure in the HRTEM images, a configuration which is very different from the hexagonal wurtzite and cubic zincblende structures found for bulk ZnO [3, 10, 11].

Studies of scanning tunneling microscopy (STM) have been carried out examining the growth of ZnO nanoparticles on Cu(111) [12]. The growth mode, size, and shape of the ZnO nanoparticles were strongly dependent on the Zn deposition temperature [12]. In a set of experiments, Zn was vapor deposited on Cu(111) or CuO_x/Cu(111) surfaces under an atmosphere of O₂ at the elevated temperatures typically used in catalytic processes for C1 conversion (550–600 K) [12, 13]. This produced large ZnO islands (300–650 nm in size), which were very rough and spread over several terraces of Cu(111); see the top of figure 1 [12]. XPS/Auger spectra indicated that these preparation conditions led to the formation of ZnO/CuO_x/Cu(111) surfaces where the oxidation state of zinc was uniform. Catalytic tests showed that the ZnO/CuO_x/Cu(111) surfaces were active for the water–gas shift (WGS; H₂O + CO₂ → H₂ + CO₂), carbon monoxide oxidation (2CO + O₂ → CO₂), and the hydrogenation of CO₂ to methanol (CO₂ + 3H₂ → CH₃OH + H₂) [4, 12–14]. A maximum of catalytic activity was observed at small coverages of ZnO below 0.3 monolayer (ML) [12–14]. When the coverage of ZnO was large, there was a decrease of catalytic activity which could be associated with a shift towards the typical catalytic properties of bulk ZnO [12–14].

In this study, the interaction of water vapor with ZnO/CuO_x/Cu(111) surfaces was investigated using synchrotron-based ambient pressure x-ray photoelectron spectroscopy (AP-XPS) and density-functional theory (DFT) calculations. Water is the main reactant in the WGS process, and its presence affects the performance of CuO–ZnO catalysts used for CO oxidation and CO₂ hydrogenation [2, 3, 5]. Our experimental and theoretical results show a strong chemical interaction between water and the ZnO/CuO_x/Cu(111) surfaces. At 300 K, the molecule dissociates on the islands of ZnO and

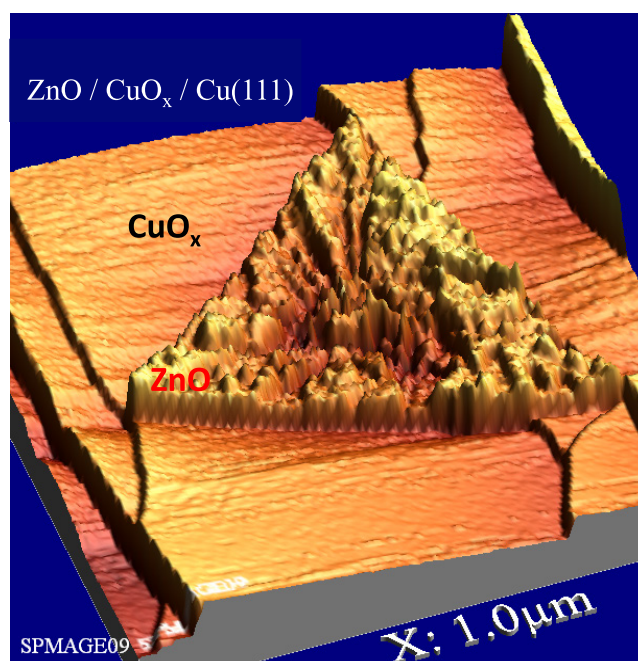


Figure 1. STM image for a ZnO/CuO_x/Cu(111) surface, $\theta_{\text{Zn}} = 0.2$ ML. The system was prepared following the methodology described in [12]. The image was collected at 1.4 V, 0.1 nA tunneling conditions. It has a size of 1000 nm × 1000 nm. A large 3D particle of ZnO is embedded on a film of Cu₂O and both are supported on a Cu(111) substrate.

can induce a ZnO → Zn_xOH transformation which affects the catalytic properties of the system.

2. Experimental methods

2.1. Photoemission and catalytic studies

Experiments of AP-XPS were performed using instruments available at the Chemistry Department of Brookhaven National Laboratory (BNL) and at beamline 9.3.2 of the advanced light source (ALS) in Berkeley. At BNL, a commercial SPECS AP-XPS chamber equipped with a PHOIBOS 150 EP MCD-9 analyzer and a Mg K α anode was used to record the Cu 2p, Zn 2p, Cu LMM, and Zn LMM regions. At the ALS, a VG Scienta R4000 HiPP analyzer was used for the XPS studies. The O 1s region was probed with a photon energy of 650 eV and a resolution of ~0.5 eV. The binding energy scale was calibrated by determining the position of the Fermi edge in valence spectra. Cycles of Ar ion sputtering and annealing (850 K, 10 min) were used to clean the Cu(111) substrate where the ZnO overlayers were grown. Islands of ZnO were deposited following a methodology described in [12]. To obtain stable overlayers of zinc oxide, zinc was vapor-deposited at a temperature of 600 K directly under an atmosphere of oxygen ($P_{\text{O}_2} \sim 5 \times 10^{-7}$ Torr) [12]. Auger electron spectroscopy (AES) was used to verify the formation of zinc oxide over the copper substrate by observing the typical lineshape of the oxide in the Zn LMM region [12, 15]. ZnO/Cu(111) surfaces were generated by exposing ZnO/CuO_x/Cu(111) systems to H₂ gas at 450 K [12]. This procedure led

to reduction of the copper oxide present in the sample without affecting the chemical state of the ZnO islands. The coverage of ZnO on the samples was determined using a combination of XPS and STM [12, 13]. The amount of OH generated on the surfaces after exposure to water was calculated using the corresponding O 1s XPS signal and comparing it to that of known coverages of chemisorbed oxygen on Cu(111) [13]. In this paper, the coverages of ZnO and OH are reported with respect to the clean Cu(111) substrate.

Catalytic tests for the WGS reaction were carried out employing a batch micro-reactor attached to a ultra-high vacuum chamber (base pressure $\sim 5 \times 10^{-10}$ Torr) equipped with instrumentation for surface characterization [13]. Using this equipment, it was possible to transfer the sample from the surface-characterization chamber to the reactor (and vice versa) without exposure to air. A combination of x-ray photoelectron spectroscopy (XPS), Auger electron spectroscopy (AES), temperature programmed desorption (TPD), low-energy electron diffraction (LEED), and ion-scattering spectroscopy (ISS) was used to characterize the ZnO/CuO_x/Cu(111) samples [12, 13]. In the experiments for the WGS testing, the ZnO/CuO_x/Cu(111) catalyst was moved into the micro-reactor at room temperature, then the reactant gases (plain H₂O or a CO/H₂O mixture) were introduced and the reaction system was heated in a range of reaction temperatures. The products of the reactions were identified and quantified by a mass spectrometer and/or a gas chromatograph [4, 13, 14]. The amount of molecules (CO₂ or H₂) generated in each catalytic test was normalized by the sample active area and the total reaction time.

2.2. Density functional calculations

A spin polarized density functional theory (DFT) implemented in the Vienna *ab initio* simulation package (VASP) code [16, 17] was used to perform the calculations. A 400 eV kinetic energy cutoff and the projector augmented wave method (PAW) [18, 19] together with the GGA exchange correlation functional plus the PBE functional [20] were employed. Monkhorst–Pack [21] meshes with $3 \times 3 \times 1$ were used to sample the Brillouin zone for all the surface calculations while meshes with $9 \times 9 \times 9$ were employed for all gas-phase species. For each reaction intermediate, calculations based on the nudged elastic band method (NEB) [22] were performed to derive the transition states.

Following our previous studies [23–25], the CuO_x/Cu(111) system was modeled by three layers of a 4×4 Cu(111) substrate and one monolayer of CuO_x, in which $x \approx 0.89$. The small and large ZnO particles observed in STM were simulated by a Zn₃O₃ cluster, Zn₃O₃/CuO_x/Cu(111) in our notation, and one full layer of wurtzite ZnO(000 $\bar{1}$), ZnO_{ML}/CuO_x/Cu(111) in our notation, supported on CuO_x/Cu(111), respectively. The Zn₃O₃/CuO_x/Cu(111) system is also useful to model Zn cations with a low coordination in a ZnO island.

For comparison, a polar ZnO(000 $\bar{1}$) surface with a wurtzite structure, represented as a six-layer slab, was also included in our study. For the surface models, the bottom two layers were fixed, and the rest were allowed to relax with the adsorbates.

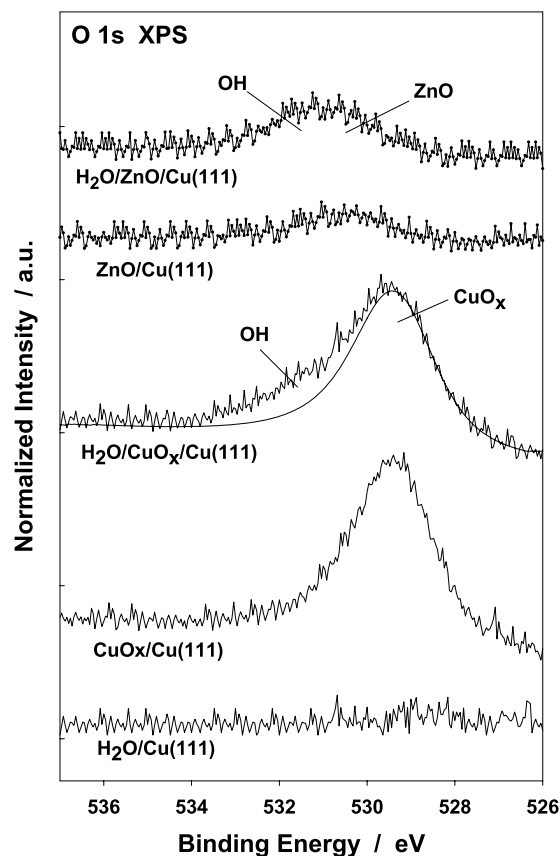


Figure 2. O 1s XPS spectra collected after exposing Cu(111), CuO_x/Cu(111) and ZnO/Cu(111) surface to 1 Torr of water at 300 K for five minutes in a batch micro-reactor. The O 1s spectra were collected after removing the water vapor from the reactor. The amount of ZnO on top of Cu(111) was close to 0.1 ML. The ZnO/Cu(111) surface was prepared by exposing a ZnO/CuO_x/Cu(111) system to H₂ gas at 450 K [12]. In these experiments, Mg K α radiation was used to excite the electrons in the photoemission process.

3. Results and discussion

3.1. XPS studies for the adsorption of water and WGS reaction activity

The rate determining step for the WGS on copper surfaces and nanoparticles is the dissociation of water [26–28]. Thus, using different approaches, we compared the dissociation of water on Cu(111), CuO_x/Cu(111), ZnO/Cu(111) and ZnO/CuO_x/Cu(111) surfaces. Figure 2 displays O 1s XPS spectra collected after exposing several samples in a batch reactor to 1 Torr of H₂O at 300 K for 5 min. In agreement with previous studies [29, 30], we found that plain Cu(111) displayed a negligible activity for O–H bond breaking at room temperature. After forming CuO_x or depositing ZnO on Cu(111), we saw a substantial enhancement in the amount of water which dissociated. In the O 1s XPS region, features were seen in the spectra around 531.5–532 eV which correspond to adsorbed OH groups [30–32]. It is known that extended surfaces of zinc oxide and copper oxide are able to dissociate water at 300 K and even at lower temperatures [33–37]. In figure 2, a copper surface with ~ 0.1 ML of ZnO clearly shows a higher reactivity towards water than plain Cu(111). In general, for

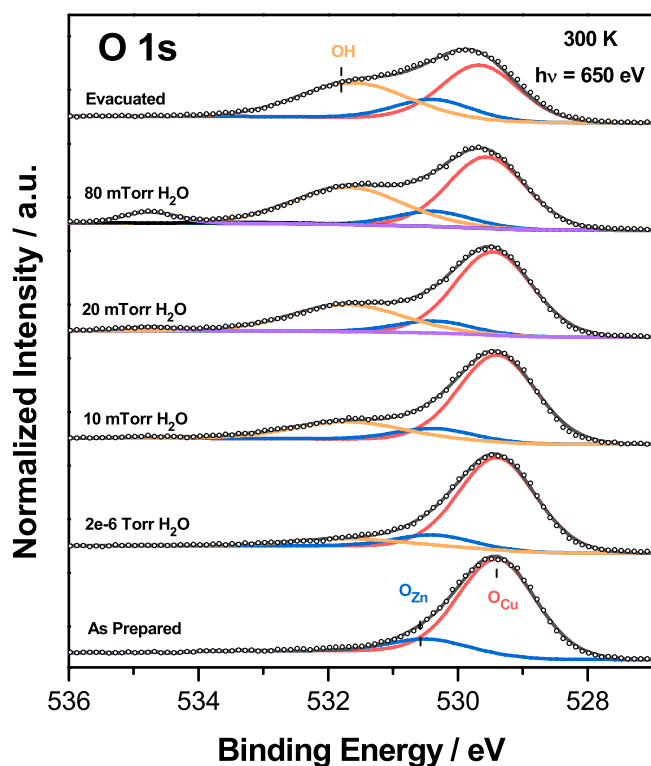


Figure 3. O 1s XPS spectra collected while exposing a ZnO/CuO_x/Cu(111) surface to different pressures of water at 300 K. The coverage of ZnO present on the CuO_x/Cu(111) substrate was ~0.2 ML. In these experiments, a photon energy of 650 eV was used to excite the electrons in the photoemission process.

the ZnO/Cu(111) and ZnO/CuO_x/Cu(111) surfaces, we saw an increase in the amount of adsorbed OH when the ZnO coverage increased from 0 to 0.8 ML. As we will see below, adsorption of water on surfaces with a ZnO coverage below 0.3 ML led to formation of chemisorbed OH on top of the ZnO islands. On the other hand, when the ZnO coverage was larger than 0.3 ML, there was evidence for the formation of Zn_xOH compounds as seen after chemisorbing water on bulk zinc oxide [33].

AP-XPS was used to study in detail the interaction of water with ZnO/CuO_x/Cu(111) surfaces. Figure 3 displays O 1s XPS spectra for a ZnO/CuO_x/Cu(111) surface under different pressures of water. With the high resolution provided by the synchrotron-based photoemission, it was possible to separate features for oxygen atoms in the oxides and adsorbed OH groups [30–32]. The data of AP-XPS show that the pressure of water has a tremendous effect of the amount of OH groups formed. Under high vacuum, at a water pressure of 10⁻⁶ Torr, the coverage of OH on the surface was negligible. When the pressure of water was raised to 80 mTorr, the coverage of OH on the surface was around 0.5–0.6 ML. Since the ZnO coverage was ~0.2 ML, the chemisorbed OH species were probably bound to copper and zinc cations present in the surface of the mixed-oxide. The OH groups were strongly bound and upon evacuation of the water from the gas phase they remained bound on the oxide surface, consistent with the *ex-situ* experiments shown in figure 2. To partially remove the OH from the ZnO/CuO_x/Cu(111) and ZnO/Cu(111)

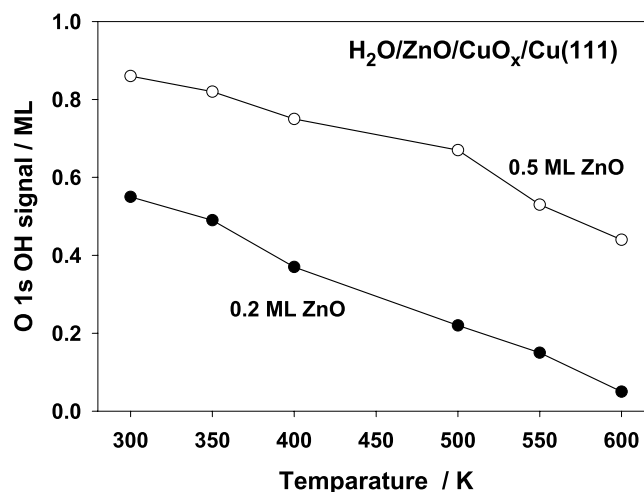


Figure 4. Effect of temperature on the O 1s XPS signal for OH groups in H₂O/ZnO/CuO_x/Cu(111) surfaces with ZnO coverages of 0.2 and 0.5 ML. Water was dosed at 300 K and the gas was removed before annealing the H₂O/ZnO/CuO_x/Cu(111) surfaces to the indicated temperatures.

surfaces, it was necessary to heat them to elevated temperatures; see figure 4. At 500–600 K, a significant coverage of OH groups was still present on the surfaces and could react with CO during the WGS process.

Figure 5 shows valence spectra collected during the AP-XPS experiments shown in figure 3. The valence region can be separated into Zn and Cu 3d features. The adsorption of water clearly induces a decrease in the intensity of the valence features for the ZnO/CuO_x/Cu(111) surface. The Zn 3d component is affected first indicating that there is preferential adsorption of water on the ZnO islands. After saturation of these islands at a water pressure of 10 mTorr, one starts to see a clear decrease in the valence features for the copper oxide. Evacuation of water at 300 K leaves OH groups of the surface of the mixed-oxide and the attenuation of the valence features remains.

As mentioned above, there was a continuous increase in the amount of adsorbed OH with an increase in the pre-coverage of ZnO on Cu(111) or CuO_x/Cu(111). For example, in figure 4, the coverage of OH deposited on the surface after dosing water at 300 K rises when going from 0.2 to 0.5 ML of ZnO. A very large amount of OH groups is present on the surface pre-covered with 0.5 ML of ZnO even after heating to 600 K. The coverage of ZnO present affected the final state of the sample. Figure 6 displays Zn LMM Auger spectra for ZnO/CuO_x/Cu(111) surfaces with 0.2 and 0.5 ML of ZnO. The initial line-shape of the Zn LMM features is that expected for ZnO [15]. In the case of the surface with 0.2 ML of ZnO (left panel), the adsorption of water and OH does not induce significant change in the line-shape of the Zn LMM features and the integrity of the ZnO nanoparticles does not change. On the other hand, for the surface with 0.5 ML of ZnO, a change in the line shape of the ZnO features is consistent with the formation of a Zn_xOH compound. Such a compound has been observed after adsorbing water on single crystal faces and films of bulk ZnO [23]. Thus, at small coverages, the isolated islands of ZnO (figure 1) have a unique behavior. At

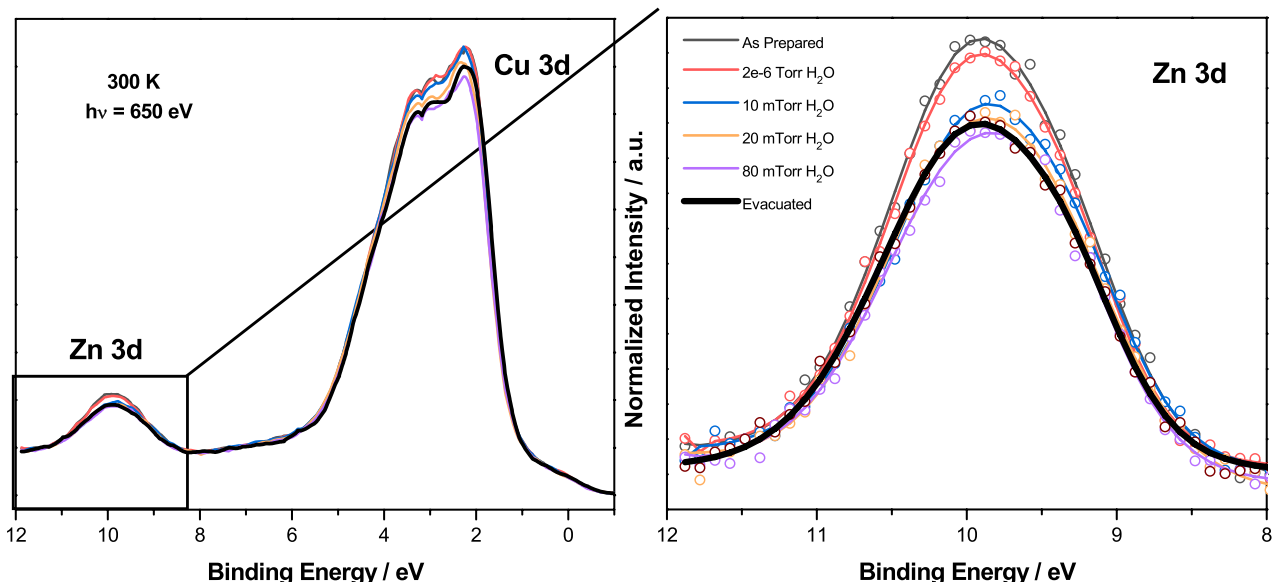


Figure 5. Valence spectra collected during the AP-XPS experiments shown in figure 3. The water pressure was increased from 2×10^{-6} to 8×10^{-2} Torr. In the final step, water was removed from the AP-XPS chamber. In these experiments, a photon energy of 650 eV was used to excite the electrons in the photoemission process.

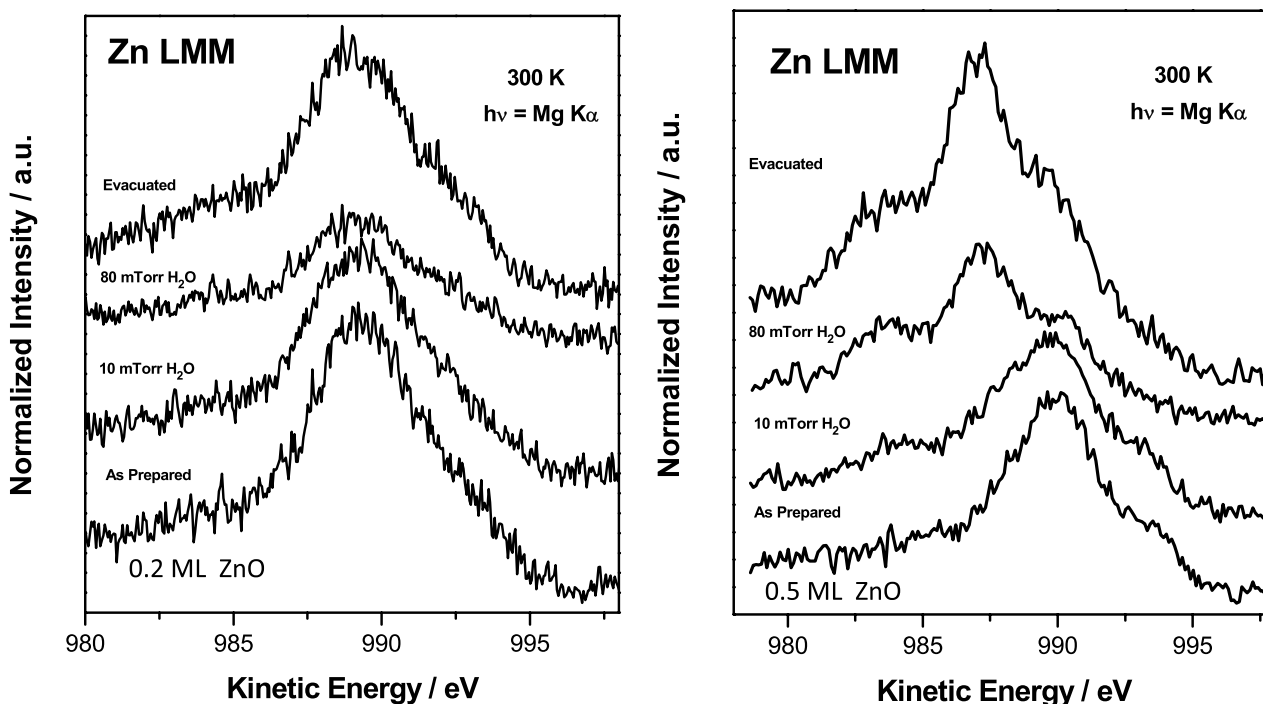


Figure 6. Zn LMM Auger spectra collected before and while exposing ZnO/CuO_x/Cu(1 1 1) surfaces to different pressures of water at 300 K. The initial coverages of ZnO were 0.2 (left) and 0.5 ML (right). In these experiments, Mg K α radiation was used to excite the electrons in the photoemission process.

large coverages of ZnO, >0.3 ML, there is coalescence of the islands and an increase in their thickness [12] with the material approaching the behavior of bulk ZnO. On the system with 0.5 ML of ZnO, the amount of OH deposited is larger (see figure 4), but the OH groups form part of a Zn_xOH compound and may not be available for the WGS process.

Figure 7 displays catalytic activities obtained for the WGS on ZnO/CuO_x/Cu(1 1 1) surfaces when the coverage of ZnO was changed ($T = 575$ K; $P_{\text{CO}} = 20$ Torr; $P_{\text{H}_2\text{O}} = 10$ Torr).

The plain Cu(1 1 1) is not very active for the dissociation of water, figure 2, and is a poor catalyst for the WGS process. The addition of ZnO increases the rate of water dissociation and the catalytic activity of the system. A maximum of catalytic activity is seen for ZnO coverages of 0.15–0.2 ML. At this point, the reactivity of the surface for the adsorption and dissociation of water is reasonable and the formed OH is not strongly bound (figure 4). At larger coverages of ZnO, things are more complicated. Post-reaction characterization with

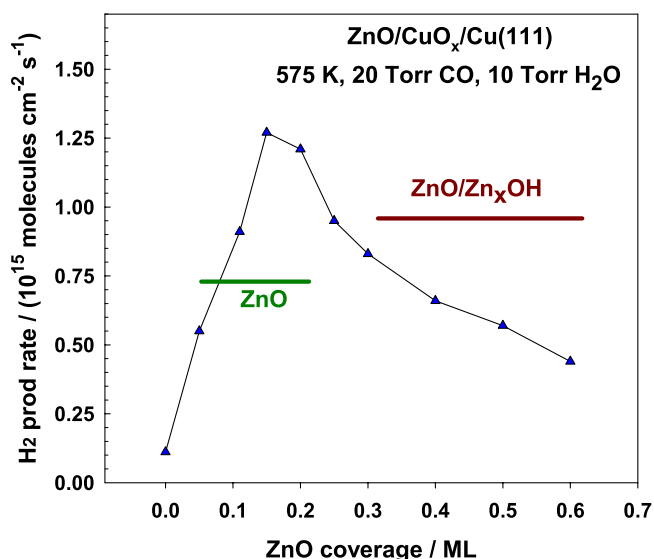


Figure 7. Rates for the water–gas shift, or production of H₂, measured on ZnO/CuO_x/Cu(111) surfaces as a function of ZnO coverage. The study was done at 575 K with 20 Torr of CO and 10 Torr of H₂O.

Zn LMM Auger spectra pointed to a ZnO → Zn_xOH transformation with the OH more strongly bound to the surface. In the C 1s XPS region, we found evidence for an increase in the formation of formates and carbonates on the surface of the catalysts. All of these factors can lead to a decrease in catalytic activity. On bulk ZnO, the OH groups react with CO to form carbonates and formates and the system is not active as a catalyst for the WGS process [4]. Thus, when dealing with a WGS catalyst with an inverse ZnO/CuO configuration, one must maintain small coverages of ZnO where the water molecule still can dissociate but the reactivity is different from that of bulk ZnO.

3.2. DFT studies for water dissociation on ZnO/CuO_x/Cu(111) surfaces

The adsorption and dissociation (H₂O + * → *H₂O → *OH + *H) of water on Zn₃O₃/CuO_x/Cu(111) and ZnO_{ML}/CuO_x/Cu(111) was studied using DFT to gain better understanding of role that ZnO plays in promoting the chemical activity of CuO_x/Cu(111). CuO_x/Cu(111) and ZnO(000 $\bar{1}$) were also included for comparison. In principle, the Zn₃O₃/CuO_x/Cu(111) system is useful to model Zn cations with a low coordination. The Zn₃O₃ cluster adopts an up-tilted motif after deposition on CuO_x/Cu(111) (see figure 8). As will be seen in the following section, the low-coordinated Zn, Zn_t in our notation, and O, O_t in our notation, atoms tilted away from the surface are unique for the small clusters and are the active sites for the water dissociation reaction. Wherein, H₂O prefer the top site of Zn_t in a tilted mode ($d_{\text{Zn-O}} = 2.17 \text{ \AA}$), where a hydrogen bond is formed between one of the hydrogen atoms and the oxygen atom ($d_{\text{O-H}} = 1.78 \text{ \AA}$) together with the stretched O_t-H bond length from 0.97 \AA in H₂O gas phase to 1.01 \AA (figure 8). Consequently, H₂O

strongly interacts with Zn₃O₃/CuO_x/Cu(111) with an adsorption energy of -0.61 eV (figure 9), which also promotes the dissociation. The O–H bond breaking on the supported Zn₃O₃ cluster is highly exothermic with the reaction energy of -0.96 eV with the corresponding barrier being as low as 0.02 eV (figure 9). The dissociation results in the hydroxylation of Zn_t and O_t sites (figure 8) as observed experimentally (figures 2 and 3). During the dissociation process, one of O–H bond length in H₂O elongates from 1.01 \AA (*H₂O) to 1.36 \AA (TS) and 2.63 \AA (*OH + *H), while the Zn_t–O (H₂O) bond length decreases from 2.17 \AA to 1.96 \AA and 1.83 \AA accordingly.

H₂O adsorption on ZnO_{ML}/CuO_x/Cu(111) is less favorable than that on Zn₃O₃/CuO_x/Cu(111) (-0.37 eV) (figure 9). This is associated with the lack of active Zn_t and O_t sites on the ZnO_{ML} motif. Although the monolayer Zn top site is preferred as in the case of adsorption on the Zn₃O₃ cluster, the corresponding lengths for the Zn–O bond ($d_{\text{Zn-O}} = 2.28 \text{ \AA}$) and O–H hydrogen bond ($d_{\text{O-H}} = 1.81 \text{ \AA}$) are longer (figure 8). A similar situation is also observed for the TS and *OH + *H states. It results in a less stable TS/dissociated state (figure 9), and thus a less exothermic reaction energy (-0.43 eV) and a slightly higher barrier (0.08 eV) compared to that of Zn₃O₃ cluster. However, both systems are more active than bulk ZnO(000 $\bar{1}$) and CuO_x/Cu(111), where the molecule is weakly adsorbed ($> -0.30 \text{ eV}$) and the dissociation is endothermic ($> 0.20 \text{ eV}$, figure 9). Furthermore, the energy barriers for O–H bond cleavage calculated on the supported ZnO systems ($< 0.1 \text{ eV}$) are much smaller than that found on CuO_x/Cu(111) ($\sim 0.8 \text{ eV}$) or those reported on Cu(111) ($> 1.0 \text{ eV}$) [26, 28, 29].

Overall, the DFT calculations are consistent with the experimental observations, showing the promoting effect of ZnO deposition on the activity towards H₂O. In figure 4, the amount of adsorbed OH generated by the dissociation of water increases when going from 0.2 to 0.5 ML of ZnO. Both ZnO/CuO_x/Cu(111) surfaces dissociate water well. The presence of ZnO can stabilize the H₂O adsorption on CuO_x/Cu(111) and greatly decrease the dissociation barrier with a moderate loading up to e.g. monolayer. However, with the overdose and the formation of a bulk-like ZnO(000 $\bar{1}$) structure, the catalyst is likely deactivated significantly when exposing to H₂O. Here we note that the activity for CuO_x/Cu(111) toward H₂O observed experimentally in figure 2 may be associated with the existence of defects, while for relatively ideal structures, as the models in the DFT calculations, a low activity was reported previously in STM studies [36, 37], which is consistent with our theoretical results. A similar situation is expected for water dissociation on ZnO(000 $\bar{1}$) [38]. Compared to the bulk ZnO(000 $\bar{1}$), the surface Zn and O sites on the supported Zn₃O₃ and ZnO_{ML} nanostructures are under coordinated when deposited on CuO_x/Cu(111) (figure 8), which enables the stabilization of adsorbed and H₂O as well as the corresponding transition states producing systems where the dissociation of water is a fast process (figure 4).

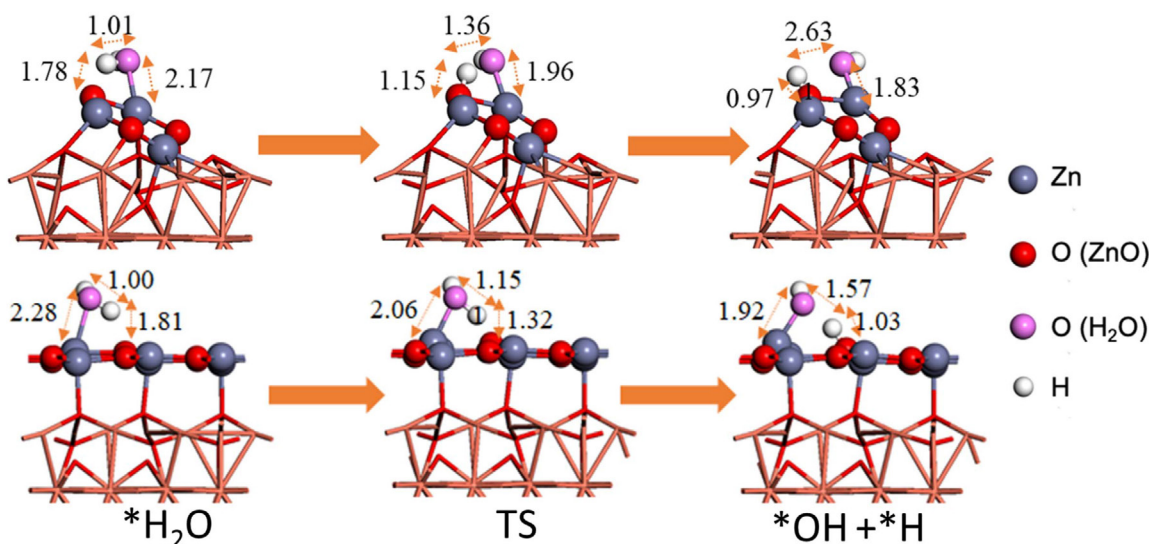


Figure 8. DFT-optimized structures for initial $*\text{H}_2\text{O}$, transition state (TS) and final ($*\text{OH} + *\text{H}$) states involved in water dissociation on $\text{Zn}_3\text{O}_3/\text{CuO}_x/\text{Cu}(111)$ and $\text{ZnO}_{\text{ML}}/\text{CuO}_x/\text{Cu}(111)$, surfaces.

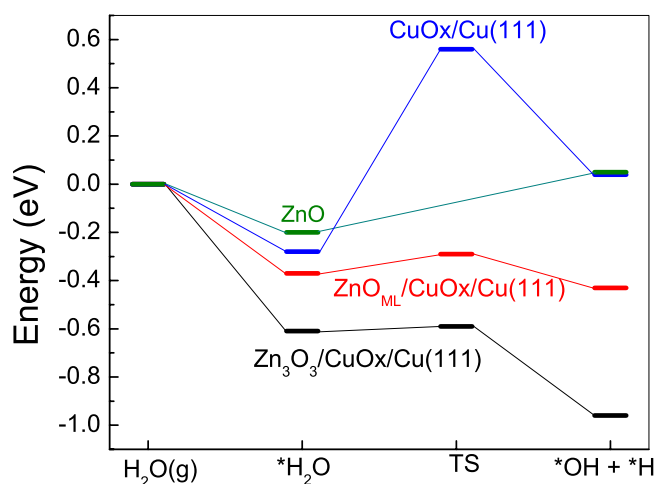


Figure 9. DFT-calculated potential energy diagrams for water dissociation on $\text{Zn}_3\text{O}_3/\text{CuO}_x/\text{Cu}(111)$, $\text{ZnO}_{\text{ML}}/\text{CuO}_x/\text{Cu}(111)$, $\text{CuO}_x/\text{Cu}(111)$ and $\text{ZnO}(000\bar{1})$ surfaces.

Conclusions

Cleavage of O–H bonds was seen with AP-XPS after depositing ZnO or generating CuO_x on a $\text{Cu}(111)$ substrate. The results of DFT calculations show a unique behavior for $\text{ZnO}/\text{CuO}_x/\text{Cu}(111)$, not seen on $\text{Cu}(111)$, $\text{CuO}_x/\text{Cu}(111)$ or $\text{ZnO}(000\bar{1})$. The presence of unsaturated Zn cations favors the dissociation of water. The $\text{ZnO}/\text{CuO}_x/\text{Cu}(111)$ system binds water well and the energy barrier for O–H bond cleavage is lower than 0.1 eV. In order to remove the OH from $\text{ZnO}/\text{CuO}_x/\text{Cu}(111)$ and $\text{ZnO}/\text{Cu}(111)$ surfaces, heating to elevated temperatures was necessary. At 500–600 K, a significant coverage of OH groups was still present on the surfaces and did react with CO during the WGS process. The final state of the sample depended strongly on the amount of ZnO present on the catalyst surface. For surfaces with a ZnO coverage below 0.3 ML, the adsorption of water did not change the integrity of the ZnO islands. On the other hand, for surfaces

with a ZnO coverage above 0.3 ML, a $\text{ZnO} \rightarrow \text{Zn}_x\text{OH}$ transformation was observed. This transformation led to a decrease in WGS catalytic activity.

Acknowledgment

The research carried out at Brookhaven National Laboratory was supported by the US Department of Energy, Office of Science and Office of Basic Energy Sciences under Contract No. DE-SC0012704. SDS is supported by a US DOE Early Career Award. P R is grateful for financial support by BID and EN-SCN. The DFT calculations used the computing resources of the Center for Functional Nanomaterials, which is a US DOE Office of Science Facility, and the Scientific Data and Computing Center, a component of the BNL Computational Science Initiative, at Brookhaven National Laboratory. This research used resources of the Advanced Light Source, which is a DOE Office of Science User Facility under Contract No. DE-AC02-05CH11231.

ORCID iDs

José A Rodríguez  <https://orcid.org/0000-0002-5680-4214>

References

- [1] Jackson S D and Hargreaves J S J (ed) 2008 *Metal Oxide Catalysis* (New York: Wiley)
- [2] Klier K 1982 *Adv. Catal.* **31** 243–62
- [3] Lunkenbein T, Schumann J, Behrens M, Schlögl R and Willinger M G 2015 *Angew. Chem., Int. Ed.* **54** 4544–8
- [4] Kattel S, Ramirez P J, Chen J C, Rodriguez J A and Liu P 2017 *Science* **355** 1296–9
- [5] Ratnasamy C and Wagner J P 2009 *Catal. Rev. Sci. Eng.* **51** 325–440
- [6] Stacchiola D J, Senanayake S D, Liu P and Rodriguez J A 2013 *Chem. Rev.* **113** 4373–90

- [7] Bond G C and Tahir S F 1991 *Appl. Catal.* **71** 1–86
- [8] Wachs I E and Routray K 2012 *ACS Catal.* **2** 1235–46
- [9] Fernández-García M, Martínez-Arias A, Hanson J C and Rodríguez J A 2004 *Chem. Rev.* **104** 4063–97
- [10] Schumann J, Kröhnert J, Frei E, Schlöl R and Trunschke A 2017 *Top. Catal.* **60** 1735–43
- [11] Schott V, Oberhofer H, Birkner A, Xu M, Wang Y, Muhler M, Reuter R and Wöll C 2013 *Angew. Chem., Int. Ed.* **52** 11925–9
- [12] Mahapatra M *et al* 2018 *J. Phys. Chem. C* **122** 26554–62
- [13] Mahapatra M *et al* 2019 *Surf. Sci.* **681** 116–21
- [14] Palomino R M *et al* 2018 *J. Phys. Chem. B* **122** 794–800
- [15] Schön G 1973 *J. Electron. Spectrosc. Relat. Phenom.* **2** 75–86
- [16] Kresse G and Furthmüller J 1996 *Comput. Mater. Sci.* **6** 15–50
- [17] Kresse G and Furthmüller J 1996 *Phys. Rev. B* **54** 11169–86
- [18] Blöchl P E 1994 *Phys. Rev. B* **50** 17953–79
- [19] Kresse G and Joubert D 1999 *Phys. Rev. B* **59** 1758–75
- [20] Perdew J P, Burke K and Ernzerhof M 1996 *Phys. Rev. Lett.* **77** 3865–8
- [21] Monkhorst H J and Pack J D 1976 *Phys. Rev. B* **13** 5188–92
- [22] Henkelman G and Jónsson H 2000 *J. Chem. Phys.* **113** 9978–8
- [23] Zuo Z, Ramírez P J, Senanayake S D, Liu P and Rodriguez J A 2016 *J. Am. Chem. Soc.* **138** 13810–3
- [24] An W, Xu F, Stacchiola D and Liu P 2015 *Chemcatchem* **7** 3865–72
- [25] An W, Baber A E, Xu F, Soldemo M, Weissenrieder J, Stacchiola D and Liu P 2014 *Chemcatchem* **6** 2364–72
- [26] Liu P and Rodriguez J A 2007 *J. Chem. Phys.* **126** 164705
- [27] Liu P 2010 *J. Chem. Phys.* **133** 204705
- [28] Gokhale A A, Dumesic J A and Mavrikakis M 2008 *J. Am. Chem. Soc.* **130** 1402–8
- [29] Fajin J L C, Illas F and Gomes J R B 2009 *J. Chem. Phys.* **130** 224702
- [30] Liu Q, Li J, Tong X and Zhou G 2017 *J. Phys. Chem. C* **121** 12117–26
- [31] Huang H H, Jiang X, Siew H L, Chin W S and Xu G Q 1998 *Langmuir* **14** 7217–21
- [32] Grinter D C *et al* 2016 *J. Phys. Chem. Lett.* **7** 3866–72
- [33] Newberg J T *et al* 2018 *J. Phys. Chem. B* **122** 472–8
- [34] Deng X *et al* 2008 *J. Phys. Chem. C* **112** 9668–72
- [35] Cox D F and Shulz K H 1991 *Surf. Sci.* **256** 67–76
- [36] Möller C and Nilius N 2017 *J. Phys. Chem. C* **121** 20877–81
- [37] Kronawitter C X *et al* 2014 *J. Am. Chem. Soc.* **136** 13283–8
- [38] Önstén A, Stoltz D, Palmgren P, Yu S, Göthelid M and Karlsson U O 2010 *J. Phys. Chem. C* **114** 11157–61